Bachelor Project

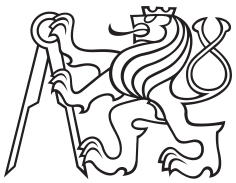

Czech
Technical
University
in Prague

F3

Faculty of Electrical Engineering
Department of Control Engineering

Quantum Mechanical Study of Diamond-based Materials for Electronic Applications

Matúš Kaintz

Supervisor: Antonio Cammarata, Ph.D.
Field of study: Cybernetics and Robotics
August 2020

Acknowledgements

I would like to thank my supervisor, Antonio Cammarata, Ph.D., for his professional guidance, everlasting patience and for instantly finding time to discuss any of my problems.

Declaration

Prohlašuji, že jsem předloženou práci vypracoval samostatně, a že jsem uvedl veškerou použitou literaturu.

V Praze, 8. August 2020

Abstract

Diamond is a very promising material for a vast variety of electronic applications. It is then worthy to study its electronic properties in order to harness them in an optimal way. In this bachelor's thesis, influences of different dopants and their concentrations on the electronic properties and geometry of diamond-doped systems have been investigated using quantum mechanical descriptions based on the Density Functional Theory. Particular importance has been given to the band gap features; to study the relevant ones, five dopants at three different concentrations were considered.

The study showed that three of the dopants (Al, B, Si) are behaving as acceptors in the diamond structure and are lowering the size of the band gap by adding acceptor states. The other two dopants (N, P) are showing metallic behaviour by eliminating band gap entirely and are adding donor energy levels to the band structure. With lowering concentration of dopant, the band gap is widening and the system is more similar to the pristine diamond.

We find a relation between the band gap and the distance between the dopant and the carbon atoms in its first coordination shell. The results will be extended by performing further analyses, which will lead to the production of scientific publications in impacted journals, as already planned.

Keywords: diamond, doping, tuning band gap

Supervisor: Antonio Cammarata, Ph.D.
Advanced Materials Group,
Department of Control Engineering,
Faculty of Electrical Engineering,
Czech Technical University in Prague,
Prague, Czech Republic

Abstrakt

Diamant je veľmi sľubným materiálom pre mnoho aplikácii v elektronike. Vďaka tomu sa oplatí skúmať jeho elektronické vlastnosti za účelom ich optimálneho využitia. V tejto bakalárskej práci bol skúmaný vplyv rôznych dopantov a ich koncentrácii na elektronické vlastnosti a geometriu diamantových dopovaných systémov za použitia kvantovo mechanického popisu založeného na teórii hustotového funkcionálu. Špeciálne sa kládol dôraz na vlastnosti zakázaného pásu. Aby bolo možné študovať, ktoré vlastnosti ovplyvňujú zakázaný pás bolo použitých päť dopantov v troch koncentráciách.

Výskum preukázal, že tri z dopantov (Al, B, Si) sa správaju v diamantovej štruktúre ako akceptory a zakázaný pás zmenšujú pridaním akceptorových stavov. Ostatné dva dopanty (N, P) ukazujú kovové správanie úplným eliminovaním zakázaného pásu a do pásovej štruktúry pridávajú energetické úrovne donora. S klasajúcou koncentráciou dopantu sa zakázaný pás rozširuje a viac pripomína čistý diamant.

Našli sme spojitosť medzi veľkosťou zakázaného pásu a vzdialenosťou medzi dopantom a najbližšími uhlíkmi. Výsledky budú rozšírené o ďalší výskum, ktorý povedie k vytvoreniu vedeckej publikácie v známych žurnáloch.

Klíčová slova: diamant, doping, ladenie zakázaného pásu

Překlad názvu: Studie materiálů založených na diamantové bázi pro elektronické aplikace z hlediska kvantové mechaniky

Contents

Figures

Tables

Chapter 1

Introduction

Semiconductors are crucial for today's society and economy. The fast technological advance requires easy adjustment to more and more harsh working conditions; in this respect, diamond is a promising material able to fulfil these requirements, thanks to its extreme properties like large thermal conductivity, electron and hole mobility, and high breakdown field strength [IHTW04]. These properties make it one of the most interesting material to be used in demanding applications such as high frequency FETs and power electronics including high power Schottky diodes [ETPG16] and switches [WB08].

Pure diamond a is wide-bandgap semiconductor with band gap of 5.47 eV [WB08]. Tuning this band gap is of primary importance for electronic applications. For this purpose, the primary objective of the thesis is to study how the presence of impurities (i.e., dopants) in the diamond structure affects the band gap size and which feature is the most significant to adjust it. In order to identify the microscopic mechanisms governing the bandgap, a great level of detail is needed. To this aim, the diamond and diamond-derived models will be based on a quantum mechanical description of the atomic interactions.

In the beginning of the thesis, I will describe the basics of the theory and the methodology used to properly quantify the electronic properties of the systems. This will be followed by suggestions on how to tune the band gap according to the results. In the study, five doping agents will be used at three different concentrations in order to study both the p-type and the n-type diamond structures.

Chapter 2

Theory and Methodology

2.1 The Schrödinger Equation

To study the electronic properties of the system that we consider, it is necessary to solve the Schrödinger equation [Sch26] which has the following formulation:

$$i\hbar\frac{\partial\Psi(\boldsymbol{r},t)}{\partial t} = H(\boldsymbol{r},t)\Psi(\boldsymbol{r},t) \tag{2.1}$$

where $\boldsymbol{r}$ is the Cartesian position in the space, t is the time, the wavefunction Ψ is the solution to be found and the Hamiltonian H represents the total energy of the system, containing the description of the atomic interactions and possible external stimuli. When the total energy, hence the Hamiltonian, does not depend on the time, Equation 2.1 reduces to the following eigenvalue-eigenvector equation:

$$H(\boldsymbol{r})\psi(\boldsymbol{r}) = E(\boldsymbol{r})\psi(\boldsymbol{r}) \tag{2.2}$$

where E is the energy eigenvalue corresponding to the eigenfunction $\psi(\boldsymbol{r})$ of the system. Since our models represent bound systems, the energy eigenvalues are quantized, that is they can assume only a discrete set of values.

Unfortunately, the analytical solution of Equation 2.2 can be found only in the case of the hydrogen atom; in all the other cases, the solution ψ and the eigenvalues must be approximated. To this aim, several methods have been developed. In what follows, I shortly mention some of them, and finally discuss which is the most suitable choice for our purposes.

2.2 The Hartree-Fock Method

The starting point to solve the time-independent Schrödinger equation is the Born-Oppenheimer approximation [BO27]. The Born-Oppenheimer approximation relies on the fact that nuclei are much heavier than electrons. According to this fact, we can fix the position of the nuclei and solve the Schrödinger equation separately for nuclei and electrons.

Then, the Hartree-Fock (HF) method is applied. It is based on averages of the inter-electron repulsion. This means that every electron is considered to be moving in the electrostatic field of the nuclei and the average field of other electrons. The Hartree-Fock method also relies on the fact that the wavefunction of the system can be separated into a set of one electron wavefunctions which are solved separately. We can finally get the whole wavefuction of the system as a product of these single electron wavefunctions (i.e., orbitals) [AF05].

2.2.1 The Self-Consistent Field

The first step of an HF calculation is the choice of the *basis set*. The basis set is a set of functions which we use to approximate the wavefuction. The precision of the results depends on the suitability of the kind and number of the chosen basis functions, the more expanded set we use the more precision we get. The most used basis functions are Slater-type orbitals, Gaussian-type orbitals and plane waves. The choice is dependent on the kind of the studied systems; the total wavefunction ψ is then represented as a linear combination of such basis functions

$$\psi = \sum_{j=1}^{M} c_j \theta_j \tag{2.3}$$

where M is the size of the basis set, θ_j is the j-th basis function and c_j is a set of coefficients calculated as a result of the iterative scheme called *Self-Consistent Field* (SCF).

At the beginning of the SCF procedure, the Fock operator is built from the Coulomb and exchange operator. The Coulomb operator includes the Coulumbic repulsion among electrons, while the exchange operator is a correction to this interaction. However, these are obtained by iterative approaches at the time of the calculation. In each iteration, a new set of

orbitals is built which is used to create a new Fock operator, the latter used as an input for the next cycle; the cycles are interrupted when the required convergence is reached.

The Fock operator is used to create the Fock matrix during; together with the overlap matrix, (i.e., the matrix formed by all the overlap integrals among the basis functions), the following eigenvector-eigenvalue equation is built:

$$\boldsymbol{FC} = \boldsymbol{SC\varepsilon} \tag{2.4}$$

where $\boldsymbol{F}$ is the Fock matrix, $\boldsymbol{S}$ the overlap matrix, $\boldsymbol{C}$ is the matrix of the coefficients in Equation 2.3 and $\boldsymbol{\varepsilon}$ is the diagonal matrix containing the energy eigenvalues. Equation 2.4 has a non-trivial solution if

$$\det|\boldsymbol{F} - \varepsilon_a \boldsymbol{S}| = 0 \tag{2.5}$$

where ε_a is the energy of the a orbital. In this way, we obtain the set of coefficients c_j. These coefficients are used for the creation of the tentative solution at the next iteration. They will be used to create new orbitals as in Equation 2.3, and therefore new matrices to feed Equation 2.5. The iterations continue until the required convergence criterion is satisfied like, for example, the total energy difference between two subsequent SCF cycles is less than a tolerance value specified in the input. The second outcome of the equation is the set ε_a of orbital energies. The sum

$$\sum_a \varepsilon_a \tag{2.6}$$

corresponds to the total energy of the electronic system and does not include the contribution coming from the repulsion among the nuclei.

2.3 Density Functional Theory

The Hartree-Fock method does not take into account the electron correlation which, indeed, it is relevant for our interests. In fact, in diamond-based systems, it has been found that the electron correlation plays a fundamental role in determining the band gap [SMH+14]. The electron correlation describes the interactions between electrons and effects their spatial distribution and the properties deriving from it. Several methods have been developed to account for this effect; some of them are known as *post-HF methods* and are based on Taylor expansions of the HF approach; however, they are computationally demanding. Among them, the most common are:

1. Configuration Interaction (CI) [DS99]

2. Møller–Plesset Perturbation Theory (MP)[MP34]

3. The Coupled-Cluster Method [Kum03]

4. Multiconfiguration Methods (MCSCF, CASSCF etc.) [SMG+12]

A convenient, less computationally demanding, alternative is represented by the Density Functional Theory (DFT)[KS65]. The Density Functional Theory is based on this observation, that the energy of the system can be expressed by a spatially dependent probability of the electron density $\rho(\boldsymbol{r})$. Following the Hohenberg-Kohn theorem formulated in 1964, the electronic energy can be written as a functional of the electron density, since there is a one-to-one correspondence between the ground state density and the electronic wavefunction of the system. Unfortunately, the theorem does not provide any information on how the energy depends on the electronic density. One year later, Kohn and Sham provided a way to express the ground state electronic density as a sum over a certain set of ψ orbitals (i.e., the Kohn-Sham orbitals)

$$\rho(\boldsymbol{r}) = \sum_{i=1}^{n} |\psi_i(\boldsymbol{r})|^2; \tag{2.7}$$

as a consequence, the ground state energy E becomes a functional $\mathrm{E}[\rho]$ of the density in Equation 2.7.

The $\mathrm{E}[\rho]$ energy functional is then written as

$$\begin{aligned} E[\rho] = &- \frac{\hbar^2}{2m_e} \sum_{i=1}^{n} \int \psi_i^*(\boldsymbol{r}_1) \nabla_1^2 \psi_i(\boldsymbol{r}_1) d\boldsymbol{r}_1 - j_0 \sum_{I=1}^{N} \frac{Z_I}{r_{I1}} \rho(\boldsymbol{r}_1) d\boldsymbol{r}_1 \\ &+ \frac{1}{2} j_0 \int \frac{\rho(\boldsymbol{r}_1)\rho(\boldsymbol{r}_2)}{r_{12}} d\boldsymbol{r}_1 d\boldsymbol{r}_2 + E_{XC}[\rho] \end{aligned} \tag{2.8}$$

where the first term is the kinetic energy of the electrons, the second term is the attraction between nuclei and electrons while the third term represents the Coulombic interaction among the total charge distribution. The fourth term cannot be computed exactly and corresponds to the exchange-correlation energy E_{XC}. By applying the results of the two theorems, the Schrödinger equation is solved by an SCF iterative scheme which is similar to that used in the case of the Hartree-Fock approach described above.

In the beginning of the calculation, an expected electron density is chosen as a tentative solution; this is usually obtained as a superposition of atomic

densities. The electron density and the chosen E_{XC} are used to to obtain the Kohn-Sham orbitals. Such orbitals are usually expressed in the form of a basis set as for the case of the HF method. With the computed orbitals, we are able to obtain a new electron density from Equation 2.7 and the ground state energy from Equation 2.8. This cycle is repeated until the required convergence is reached.

2.3.1 Exchange–Correlation Functionals

As we mentioned above, the E_{XC} functional cannot be computed exactly and several formulations of it exist. The choice of the proper formulation is done by making preliminary tests. The tests are based on trying different formulations: the results are compared with known experimental data whenever available, and the formulation giving the best agreement is selected. Usually, the studied structures are known experimentally; in this case, the main benchmark is the comparison between the calculated and the experimental atomic geometry. Once the specific form of E_{XC} is chosen, it is specified as an input of the simulation and remains unchanged throughout the calculation.

The Local Density Approximation is the most simple approach to obtain the functional form of E_{XC}. It relies on the electron density and the exchange-correlation energy ε_{XC} per electron of the homogeneous electron gas as an approximation.[AF05] The *homogeneous electron gas* is a model in which electrons travel through a space of infinite volume with a uniform distribution of the positive charge. While this approximation works well for most of the systems [AF05], its accuracy is getting worse with systems containing larger number of molecules.[AF05] In such cases, an improvement of the LDA description is used, namely the Generalized Gradient Approximation (GGA). The GGA is based on the LDA approach and adds a gradient correction to the electronic density. In the practise, the exchange-correlation energy is usually split into exchange and correlation parts and various approaches to get the former can be mixed with other approaches to get the latter. Other sophisticated methods to obtain a more precise description of the E_{XC} functional exist, these including the *meta-generalized gradient approximation* (MGGA)[JA16], which also involves the second derivative of the electron density, and *hybrid functionals* which combine the Hartree-Fock and/or other E_{XC} LDA or GGA descriptions (e.g., B3LYP [Bec93]).

2.4 Crystal Structure

The geometric description of our model systems relies on the concept of *crystal structure*. A crystal structure is made by periodic repeating atomic arrangements. The main properties defining a crystal structure are:

1. **The basis**, the geometric arrangement of the atoms forming the repetition unit;
2. **The Space/crystal lattice**, the set of mathematical discrete points (the "net"), defined by linear combinations of the kind $\boldsymbol{r} = u_1\boldsymbol{a}+u_2\boldsymbol{b}+u_3\boldsymbol{c}$ where $\boldsymbol{a}$, $\boldsymbol{b}$ and $\boldsymbol{c}$ are the lattice vectors defining the unit volume;
3. **Space Group**, the set of geometric symmetries owned by the basis.

The periodic repetition of the basis through the definition of the crystal lattice determine the space group, and are specified as an input of the simulations.

2.4.1 Bravais Lattice and Primitive Cell

With the term *Bravais lattice* we refer to possible distinct repetitions in the space of points corresponding to an atom or group of atoms in a crystal. In the three-dimensional case, there are 14 Bravais lattices divided into 7 lattice systems. The Bravais lattice relevant for our study is the face-centered cubic (FCC). It consists of lattice points located at the corners of a cube and in the middle of each face. The FCC lattice is the kind of lattice which describes

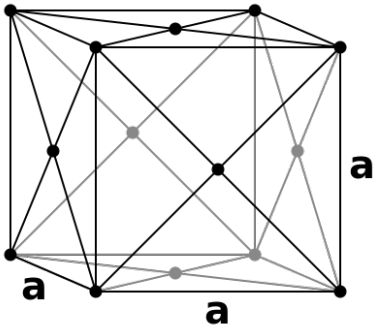

Figure 2.1: Face centered cubic (FCC) Bravais lattice. [Wik07]

the diamond structure, which is the target of our studies.

To each point of the Bravais lattice it is possible to associate a certain set of atoms arranged in the space in such a way that they reproduce the whole crystal structure; in this way we build the *unit cell*. The *unit cell* is then defined as that volume the infinite replicas of which are able to completely tile the whole space. If the volume of the unit cell is one of the smallest that can be obtained, the unit cell is said to be *primitive*. Many different primitive cells can be built, according to the set of construction rules that are chosen; the most common kind of primitive cell is the *Wigner-Seitz* cell [Kit71].

The unit cell may contain symmetry elements such as rotations, rototranslations (screw axes), inversion, reflection etc. If the translation operations are combined with such symmetry operations, we obtain what is called the *space group* [Gia92]. The number of all the possible three-dimensional space groups amount to 230, each uniquely identifying the set of symmetries owned by the system.

2.4.2 Reciprocal Lattice and Brillouin Zone

When we want to study periodic systems, it is convenient to consider the Fourier transform of the physical properties (e.g., the electronic density). To this aim, from the unit cell describing the system in the Cartesian space, we can define the *reciprocal lattice* in the *reciprocal* space as the Fourier transform of the Bravais lattice in Cartesian space. Accordingly, we will refer to the starting unit cell as *real* or *direct* lattice. If the unit cell of the real space is primitive, the unit cell of the reciprocal space is also primitive and it is called *first Brillouin zone*. The reciprocal lattice contains the same set of symmetry operations of the real lattice. Each Brillouin zone then contains *high-symmetry points*, that are special positions in the reciprocal space space to which there are associated several symmetry operations. Since the Hamiltonian is invariant under the same set of symmetry operations, the solution of the Schrödinger equation will also have the same symmetries. This constitutes an advantage because it is enough to evaluate the wavefunction only at a limited set of points in the reciprocal space; the full solution will then be built by applying the symmetry operations to the obtained wavefunction. In this way, the computational load is drastically reduced compared to the case of the evaluation of the solution in the full Brillouin zone. Moreover, by exploiting the symmetries, each Brillouin zone can be described by a minimal volume called *irreducible Brillouin zone* (IBZ). To further reduce the computational load, it is then enough to consider only the IBZ and build the full solution according to the symmetries of the system.

The Brillouin zone of our interest is represented in Figure 2.2, and it is

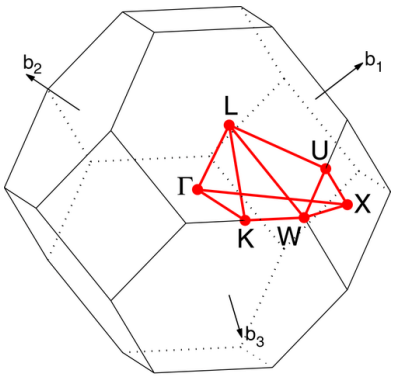

Figure 2.2: Schematic representation of the Brillouin zone of the FCC lattice. Reproduced from Ref. [SC10].

the reciprocal lattice of the FCC structure adopted by the diamond-based systems which we will discuss later on.

2.5 The Bloch's Theorem and the Electronic Structure

The periodicity of the crystal structure implies the periodicity of the interatomic potential. For periodic potentials, Felix Bloch proved that the solution of the Schrödinger equation has the form

$$\psi_k(\boldsymbol{r}) = u_{\boldsymbol{k}}(\boldsymbol{r})e^{i\boldsymbol{k}\cdot\boldsymbol{r}} \tag{2.9}$$

where $\psi_k(\boldsymbol{r})$ is the one-electron Bloch function or Bloch wave, which is an eigenfunction of the Hamiltonian, $\boldsymbol{k}$ is a vector of the reciprocal lattice and $u_{\boldsymbol{k}}(\boldsymbol{r})$ is a periodic function with the same period of the crystal lattice. Wavefunctions of the kind in Equation 2.9 can be seen as a wavefunction $e^{i\boldsymbol{k}\cdot\boldsymbol{r}}$ describing a free electron multiplied by a periodic modulation.

The Bloch's functions in Equation 2.9 are identified (i.e., *labelled*) by the vectors $\boldsymbol{k}$ and similarly the correspondingly eigenvalues. Since we are treating confined systems, at each $\boldsymbol{k}$ vector, there corresponds a discrete set of possible eigenvalues, that is, of possible energy values or *levels*. The set of different energy values realized at varying $\boldsymbol{k}$ vectors constitute what is called the *electronic band structure*, which is a characteristic of the system. From the band structure, we can determine the electronic properties of the system.

An important quantity related to the band structure is the Fermi level, which is defined as the energy level, if it exists, with probability of 50 % to

be occupied by one electron at a certain finite temperature. According to the position of the Fermi level with respect to the energy levels, the material is found to be conductive or insulating. In the former case, the Fermi level lies within an almost continuous set of bands. Since the set of allowed energy values is discrete, it is possible that there are energy ranges within which no energy levels can be realized; each of such range is called *band gap*. If the Fermi level lies within a bandgap or at its lower limit, the material shows semiconductor or insulating properties. The *valence band* is the uppermost set of energy levels which is fully occupied by all the electrons of the systems at absolute zero temperature. The *conduction band* instead corresponds to the set of energy levels associated to wavefunctions describing electrons that can move across the material. The energy gap between the highest energy value of the valence band and the lowest energy value of the conduction band is the most common band gap studied in solid state systems. For our purposes, we focus on the energy range including the valence and conduction bands, then the Fermi level.

A useful quantity derived from the set of allowed energy values is the *density of states*, defined as the number of states (i.e., eigenfunction) allowed within an energy range $[E, E + dE]$, where dE tends to zero. The density of states then provides a quick way to quantify the band gap around the Fermi level, if any, and the possible overlap among the bands.

2.6 Used Software

To solve the time independent Schrödinger equation and calculate the physical properties of our interest, we make use of the ABINIT package [GAA+20]. In order to achieve our goal, that is to study how to control the band gap in diamond-based systems, we first need to obtain the ground state geometry of our models. After we obtain it, we then proceed in the analysis of the corresponding electronic structure and finally discuss what are the relevant parameters to control the band gap.

The ABINIT software exploits the density functional theory to calculate the properties of the studied materials. The basis set used to expand the electron wavefunction is made by plane waves of the kind $e^{i\boldsymbol{k}\cdot\boldsymbol{r}}$, which is a computationally efficient choice to represent the Bloch functions. On the other hand, the plane waves loose their efficiency when describing the wavefunctions near the nucleus. To overcome this issue, *ad hoc* descriptions, namely *pseudopotentials*, are used [SBv+11]. By using the pseudopotentials, the number of basis functions can be reduced and limited to the description

of the electrons in the valence band, whenever the core electrons do not play a decisive role in determining the physics of the system under study.

2.6.1 Calculation of Ground State Geometry

The steps to obtain the ground state geometry of a model system can be summarized as follows. As an input, a tentative geometry is provided, together with a suitable choice of the Hamiltonian and other technical parameters. The total electronic energy is calculated via the SCF procedure as in subsection 2.2.1. Once the ground state electronic density has been obtained, the forces acting on the atoms are calculate by applying the *Hellmann-Feynman theorem* [Fey39]. If the maximum value among all the components of all the forces is smaller than a chosen threshold parameter, the geometry is considered stable and the geometric optimization terminates. On the contrary, if the forces are larger than the threshold, the positions of the nuclei are modified in such a way to minimize the total energy (e.g., displacing the atoms along the direction of the energy gradient), and the SCF procedure is repeated.

Chapter 3

Doped-diamond Systems

The starting point of our simulations is the pristine structure of the pure diamond obtained from diffraction data[BSW$^+$14]. In order to find the optimal set of simulation parameters, we optimize the experimental structure at different energy functionals, k-mesh sampling, and plane-wave cutoff among others; we also tested the parallelization options available in the ABINIT package so as to obtain the largest parallel scaling possible and reduce the simulation time. In Table 3.1, we report the specifics of the relaxed pure diamond geometry, while the optimal simulation parameters are the following: *i*) WC energy functional[WC06], *ii*) $11 \times 11 \times 11$ Monkhorst-Pack k-mesh [MP76] ($21 \times 21 \times 21$ for the undoped structure, $5 \times 5 \times 5$ for the models with the largest size), *iii*) 1633 eV plane-wave energy cutoff, *iv*) 3265 eV energy cutoff for the PAW double grid, *v*) 10^{-10} eV tolerance on the energy difference to stop the SCF cycles, *vi*) 5×10^{-6} eV/Å tolerance on the maximum component of the forces on the atoms to stop the geometry optimization.

Space group	$Fd\bar{3}m$ (227)		
lattice parameters	$a = b = c = 3.56123$ Å		
lattice angles	$\alpha = \beta = \gamma = 90.0°$		
asymmetric unit	x	y	z
C	0.0	0.0	0.0

Table 3.1: Optimized structural parameters of the pure diamond model geometry.

To study how the presence of dopant atoms change the electronic properties of the pure diamond, we consider five different kind of dopants, namely B, Al, Si, N and P. The boron and aluminium atoms are *electron acceptors*: since they have less valence electrons than the carbon atom, they make the diamond structure of *p-type*. The nitrogen and phosphorus atoms are instead *electron donors*: they have more valence electrons than the carbon atom, thus creating what is known as *n-type* diamond. Silicon atom has the same number of valence electrons as the carbon atom; however, as we will see, it shows the same properties of the acceptor atoms. The doped structures are built by replicating the unit cell of the pure diamond, thus obtaining *supercells* of different size; we then substitute one of the carbon atoms with one dopant atom. We consider $2 \times 2 \times 2$, $3 \times 3 \times 3$ and $4 \times 4 \times 4$ supercells containing 16, 54 and 128 atoms, respectively, containing only one dopant atom. In this way, we simulate a dopant concentration of 6.25 %, 1.85 % and 0.78 %. As

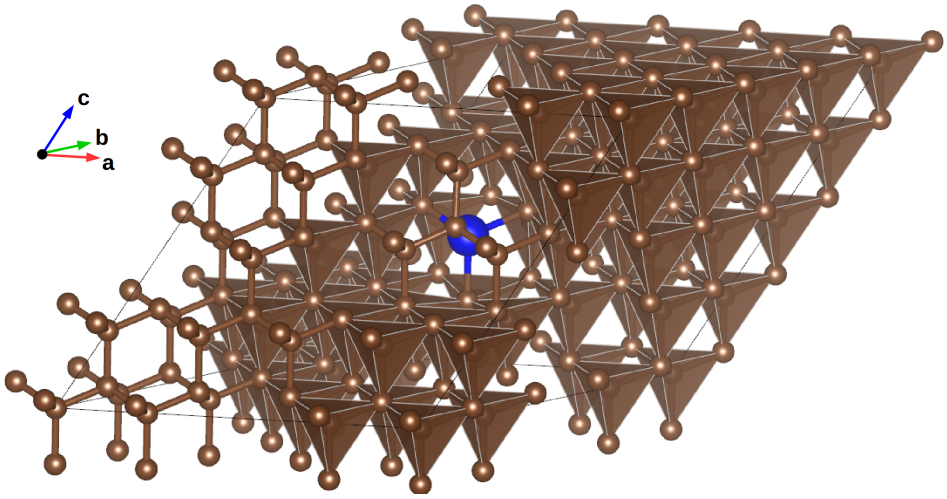

Figure 3.1: Example of primitive unit cell simulating a dopant concentration of 0.78 %. The blue sphere represents the dopant atom while the brown spheres indicate the position of the carbon atoms. The figure has been created with the aid of the VESTA[MI11] software.

an example, in Figure 3.1 we report the geometry of the primitive unit cell used to simulate a dopant concentration of 0.78 %.

3.1 Geometry analysis

The most apparent effect of the presence of a dopant in the diamond structure is the change of the atomic geometry with respect to the pristine structure. Irrespective of the atomic type of the dopant and irrespective of the doping concentration, each atom in the structure is surrounded by four atoms (*first*

neighbours) arranged in such a way to form a tetrahedron (see Figure 3.1). Since such tetrahedra are regular, the distances between an atom and each of its first neighbours are the same no matter if the coordinating atom is a carbon atom or a dopant one. For this reason, in order to quantify the change induced in the undoped structure, we consider only the X–C and the C–C bond lengths, where X is the dopant atom; the data is reported in Table 3.2.

X	concentration [%]	X–C [Å]	C–C [Å]	unit cell volume [Å^3]
Al	6.25	1.773	1.588	101.07
	1.85	1.786	1.552	313.06
	0.78	1.788	1.545	727.62
B	6.25	1.583	1.548	91.65
	1.85	1.582	1.542	304.45
	0.78	1.581	1.541	719.15
N	6.25	1.599	1.544	90.81
	1.85	1.592	1.540	303.75
	0.78	1.588	1.538	718.44
P	6.25	1.693	1.575	98.54
	1.85	1.700	1.552	311.23
	0.78	1.701	1.543	725.96
Si	6.25	1.716	1.583	99.41
	1.85	1.723	1.552	311.81
	0.78	1.726	1.543	726.39
C	6.25			90.33
	1.85	-	1.542	304.86
	0.78			722.64

Table 3.2: Interatomic distances and cell volume of the model systems. In the last line, the data relative to the undoped structure are reported; the concentration values for the undoped structure refer to the unit cell size used for the doped model, and the corresponding volume values are reported to facilitate the comparison.

As expected, we find that dopant atoms with larger atomic radius induce larger distortions into the ion coordination environment, the largest ones found in the structures doped with aluminum. An exception is represented by the nitrogen atom: with respect to the boron doping case, nitrogen induces larger distortions despite it has a smallest radius. At lowering concentrations, the X–C distances are changing only by a small amount, whereas at 1.85 % and the 0.78 % doping the distances are mostly the same; at the same time, the C–C distances approach those found in the pure diamond when they are measured far from the dopant atom. Interestingly, in the cases X = B, N the C–C distances farther from the dopant are almost the same as in the pure diamond structure even at higher concentrations. We can then conclude that the dopant has no influence on the geometric structure if the concentration is low enough that between two dopant atomic sites there are at least three

C-coordination shells. The volumes of the cells are directly influenced by the interatomic distances. Finally, we observe that the cell volume of the doped structures is more and more similar to the undoped case at decreasing concentrations; this is indeed an expected behaviour, since the dopant induces isotropic distortions into the coordination tetrahedron environment, thus leaving unaltered the lattice angles.

3.2 Electronic Structure analysis

We now analyse the effect of the p- and n-doping. First, we discuss the influence of the dopant type on the band gap, the band structure and the density of states, and compare it with the corresponding quantities of the pure diamond. We then analyse how the concentration affects the abovementioned properties.

3.2.1 p-type Doping

In the present section, we include silicon together with the boron and aluminum atoms among the p-type dopants, as it shares similar features with the latter two ones.

We start by comparing the band structures obtained in the systems with concentration equal to 6.25 % (Figure 3.2); similar behaviour is found for the p-doped systems at the remaining concentrations. We observe that all the p-doped models display band gaps narrower than that found in the pure diamond. In the majority of the cases, the band gap size is increasing with lowering concentration, approaching the value found in the undoped diamond; we report these values in Table 3.3. The largest change is observed in the aluminium doped system. The calculated band-gap widths suggest that the p-doped structures should show semiconducting properties.

In order to understand the origin of the different band gap values between the undoped and the p-doped systems, we calculate the atom-projected density of states and show them in Figure 3.3. We here recall that the dopant atoms are electron acceptors. The electron occupying the top of the valence band of the pristine structure is transferred to the dopant once it substitutes for one carbon atom. Consistently, we find that the dopant contributes mostly to the top of the valence band with its own states, irrespective of the kind of

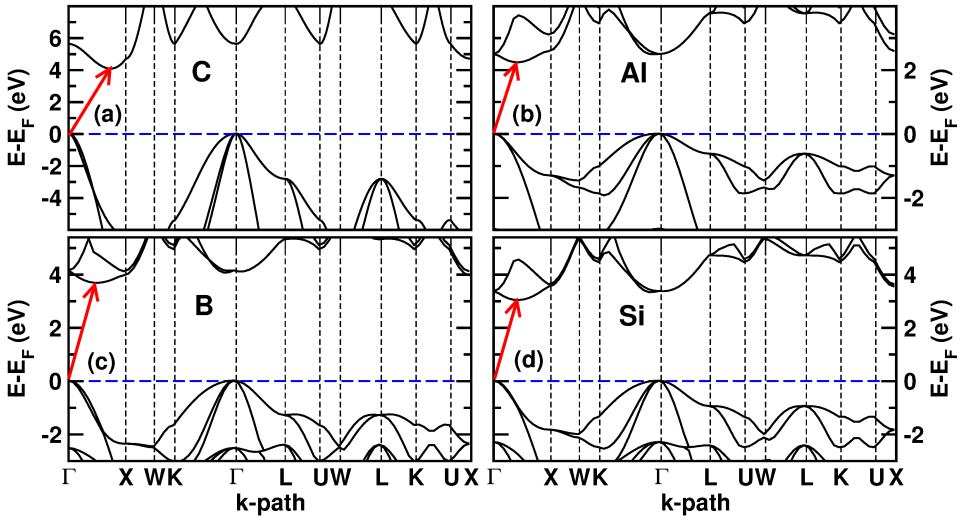

Figure 3.2: Electronic band structure of (a) pure diamond, (b) Al-doped, (c) B-doped and (d) Si-doped structures at 6.25 % concentration. The band structure is calculated along a standard piece-wise linear path joining the high symmetry points in the irreducible Brillouin zone (see Figure 2.2). The optical gap is calculated as the vertical electronic transition with the corresponding lowest energy, and it is found to occur at the Γ point, irrespective of the chemical composition; the red arrow indicates the transition corresponding to the fundamental band gap.

dopant. This induces a readjustment of the whole energy level spectrum, the Fermi level is shifted and the band gap is narrowed.

We continue our analysis by comparing the density of states at different concentrations; we report such comparison in Figure 3.4. The largest effect is found in the case of the aluminum doping, while larger concentrations narrow the band gap significantly. Interestingly, while the Si-doped and Al-doped structures show similar behaviour, the B-doped system is less affected by the change in the concentration.

3.2.2 n-type doping

We continue our analysis by considering the n-type systems. We calculate the band structures along the same k-path of the irreducible Brillouin zone that we used in the case of the p-type compounds; the results are reported in Figure 3.5. We find that the n-type dopants shift the Fermi level above the bottom of the conduction band as correspondingly calculated for the undoped diamond. This is an expected behaviour. As a first approximation, we can imagine that the pristine band structure has to accommodate the

X	concentration [%]	optical band gap [eV]	fundamental band gap [eV]
Al	6.25	2.47	2.28
	1.85	3.21	3.21
	0.78	3.86	3.64
B	6.25	4.04	3.73
	1.85	3.93	3.93
	0.78	4.26	4.04
Si	6.25	3.32	3.08
	1.85	3.81	3.81
	0.78	4.25	3.99
-	-	5.67	4.14

Table 3.3: Band gap values of p-type doped structures. In the last line, the values relative to the pure diamond are reported.

extra electron coming from the donor atom; the available levels with the lowest energy are those located at the bottom of the conduction band. The extra electron is then accommodated in these levels and the Fermi level is shifted up in energy in correspondence with the new last occupied level. Since the Fermi level now lies within a band, the compound is metallic. In this case, we do not therefore find an electronic band gap relevant for the electronic conduction, as the Fermi level is crossing the conduction band; this makes the n-doped materials conductive. Finally, we notice that a band gap still exists below the Fermi level within the valence band, such gap resembling that of the insulating p-doped structures.

We now consider the density of states, in order to understand what is the contribution of the energy levels of the donor atom and how they make the band gap disappear; we report them in Figure 3.6. We observe that the profile of the total DOS of the doped structures is close to that of the pure diamond; at the same time, the top of the valence band is mainly formed by the states associated to the donor atom. This is consistent to what we discussed above: the effect of substituting one carbon atom with a donor one is to add one electron to the bottom of the conduction band of the pristine structure, making the latter metallic while almost preserving the original energy level spectrum.

3.3 Discussion

The results presented above suggest that the presence of a dopant atom in the diamond structure does not alter the features of the electronic band dispersions or the profile of the density of states; in fact, the pristine structure

is able to accommodate the change of the number of electron without altering the relative energy distribution of the band levels. The main effect is instead to change the position of the Fermi level: acceptor dopants modulate the width of the band gap while donor atoms close the band gap making the system metallic. We notice this behaviour irrespect of the dopant concentration; indeed, the latter has the role to modulate the effect of the atomic type on the position of the Fermi level.

To parameterize how the atomic type determines the width of the band gap, we need to choose a physical feature which quantifies both the kind of atom and the environment in which it is embedded. To this aim, we consider the X–C distance at different concentrations and relate it to the band gap of the system (Figure 3.8). We notice that, in general, at constant concentration, the larger the distance between the dopant and the first neighbour carbon atom, the smaller the fundamental band gap. The optical gap instead appears to be less sensitive to the X–C distance, still showing a similar trend. On the contrary, at constant dopant atomic type, we observe that an increase of the X–C distance produces an increase of the band gap. Larger distances arise in correspondence with dopant atoms with larger atomic radii. However, the atomic radius is not a convenient parameter if we want to compare the results at different concentrations when the atomic type is unchanged. For this reason, we believe that the X–C distance is a more effective descriptor. These observations suggest that acceptor atoms inducing larger distances than those here reported might generate corresponding narrower band gaps at constant concentrations; correspondingly, they might induce larger band gaps when realized at a constant atomic type. Further investigations on the effect of variable X–C distance at constant dopant atomic type and unit cell volume will provide a better parametrization of the electronic band gap in terms of the geometric properties of the system.

Finally, we here want to notice that the present results constitute the starting point for further studies, in which analyses on the subtle features of the electronic structure at different dopant atomic type will provide more complete information on how to tune the electronic band gap. Indeed, such analyses are already ongoing and will be part of a planned publication in an impacted scientific journal.

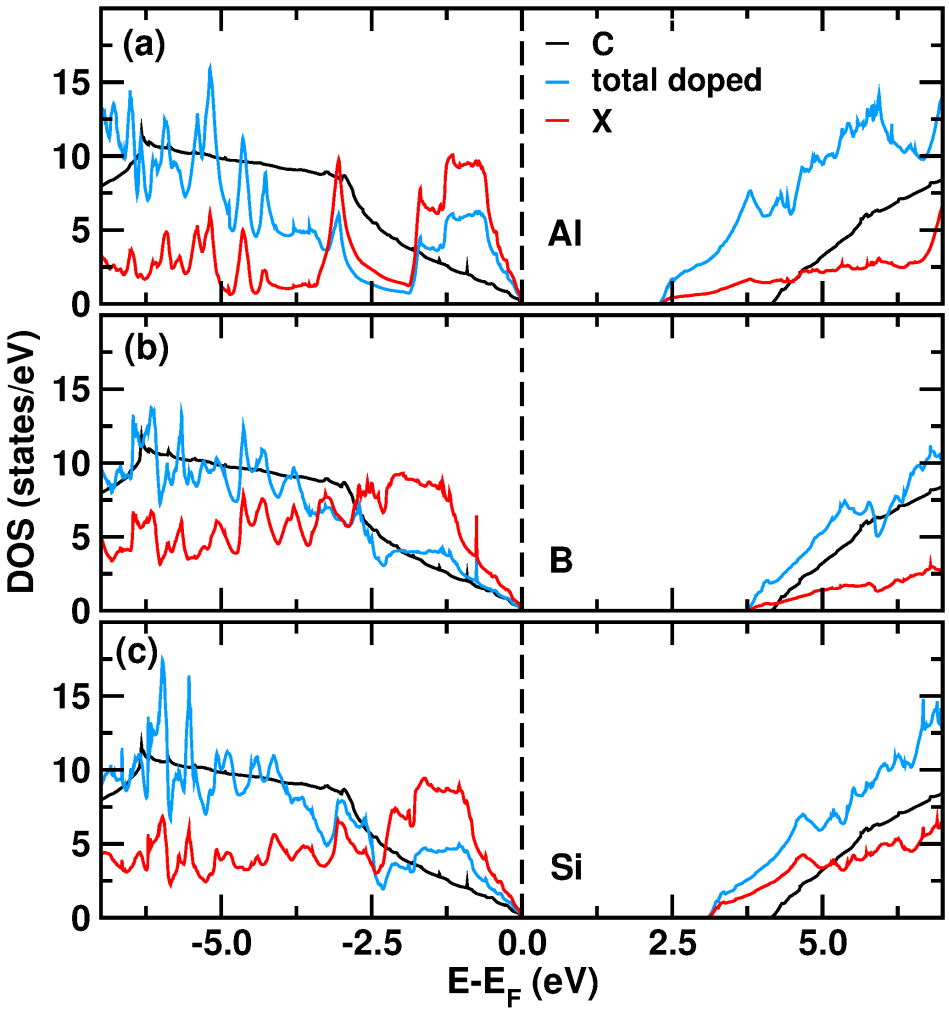

Figure 3.3: Electronic density of states calculated for p-doped systems at concentration equal to 6.25 %. The "C" and "total doped" labels indicate the total density of states of the pure diamond and the doped system, respectively, while the "X" label indicates the density of states projected on the atomic site of the dopant corresponding to the atomic symbol in the plot. For clarity of presentation, in each plot, the total DOSs' are normalized by the number of atoms in the unit cell while the projected DOS are reported as calculated. The Fermi level is set at 0.0 eV and is indicated by the vertical dashed lines.

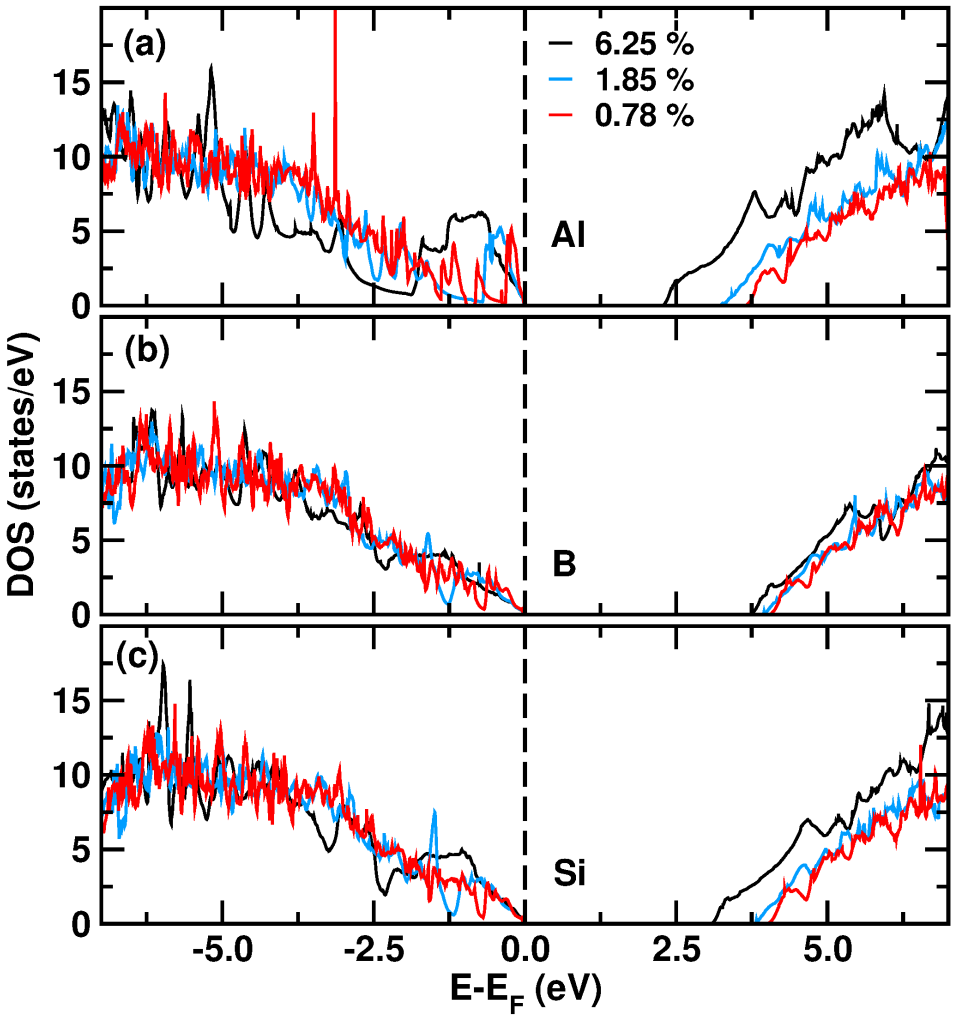

Figure 3.4: Total electronic density of states of (a) Al-doped, (b) B-doped and (c) Si-doped systems calculated at the considered dopant concentration values. The data have been normalized by the number of atoms. The Fermi level is set at 0.0 eV and is indicated by the vertical dashed lines.

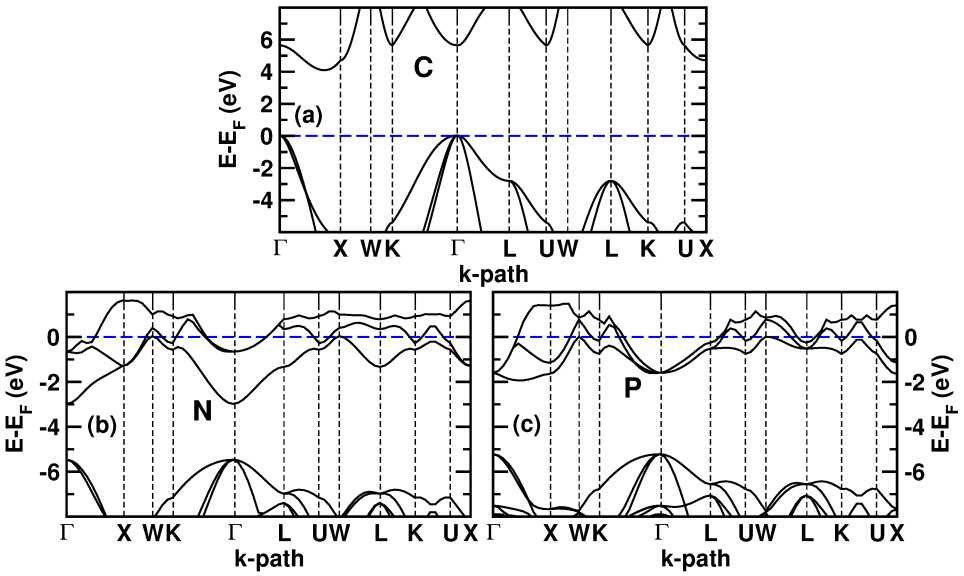

Figure 3.5: Electronic band structure of (a) pure diamond, (b) N-doped and (c) P-doped structures at 6.25 % concentration. The band structure is calculated along a standard piece-wise linear path joining the high symmetry points in the irreducible Brillouin zone (see Figure 2.2). The Fermi level has been set to 0.0 eV and is indicated by the dashed lines.

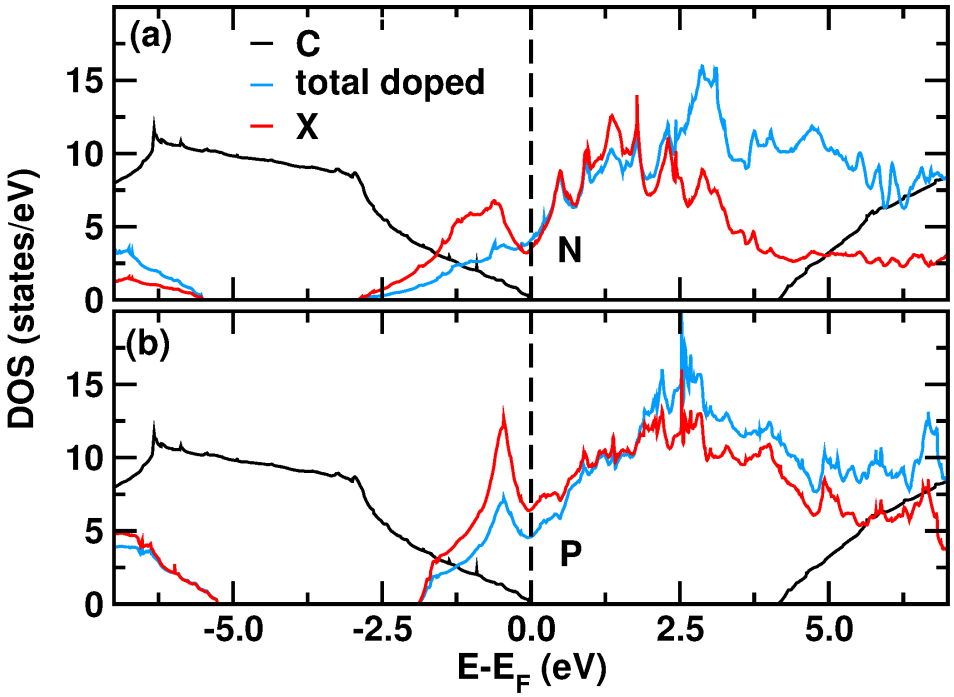

Figure 3.6: Electronic density of states calculated for n-doped systems at concentration equal to 6.25 %. The "C" and "total doped" labels indicate the total density of states of the pure diamond and the doped system, respectively, while the "X" label indicates the density of states projected on the atomic site of the dopant corresponding to the atomic symbol in the plot. For clarity of presentation, in each plot, the total DOSs' are normalized by the number of atoms in the unit cell while the projected DOS are reported as calculated. The Fermi level is set at 0.0 eV and is indicated by the vertical dashed lines.

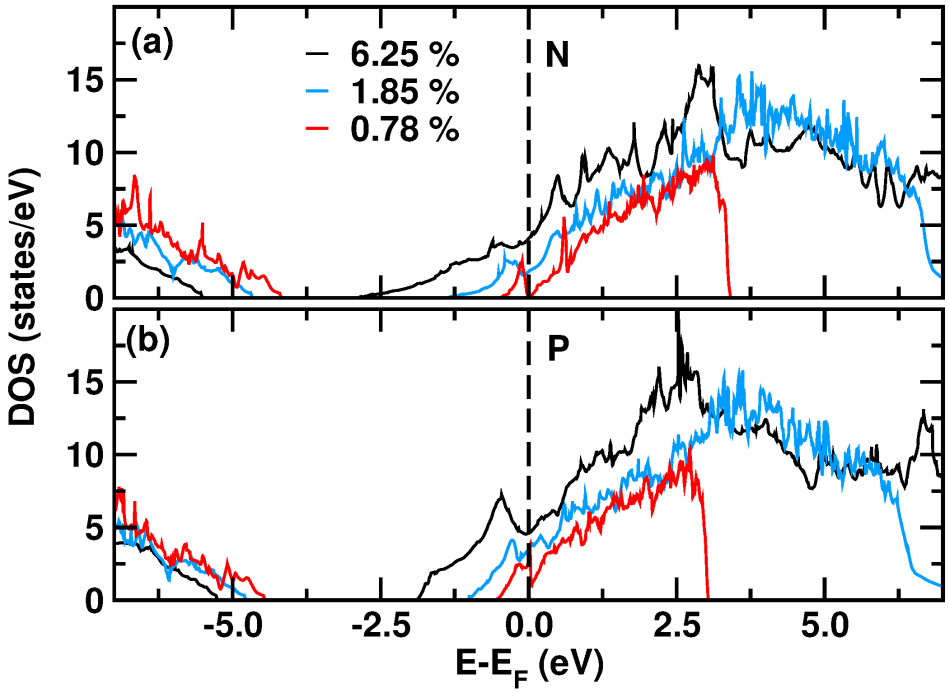

Figure 3.7: Total electronic density of states of (a) N-doped and (b) P-doped systems calculated at the considered dopant concentration values. The data have been normalized by the number of atoms. The Fermi level is set at 0.0 eV and is indicated by the vertical dashed lines.

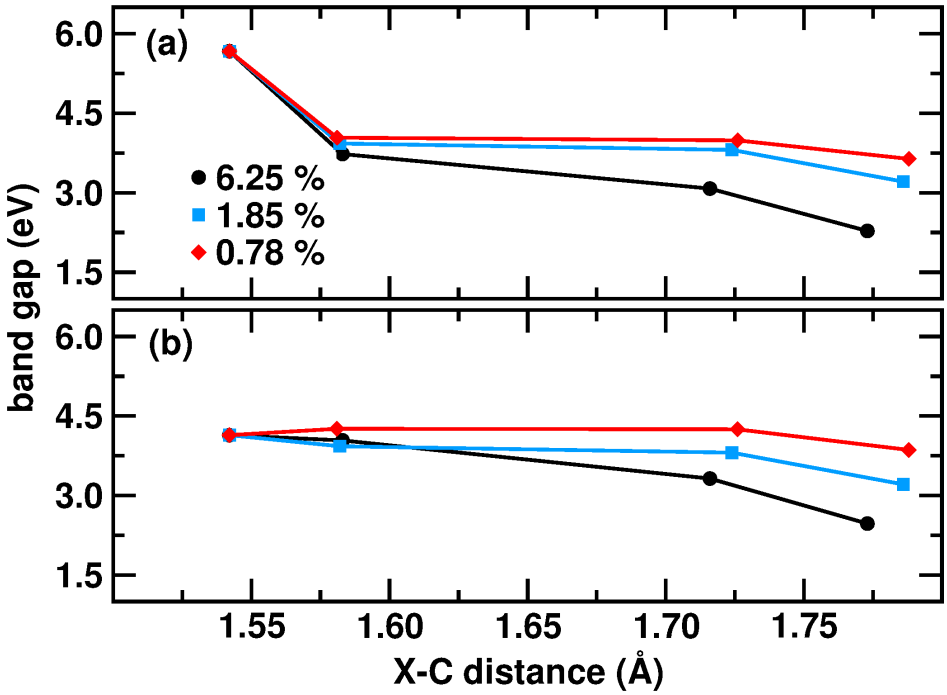

Figure 3.8: (a) Optical and (b) fundamental band gap calculated for the p-doped systems as a function of the X–C distance at the considered concentrations. The value of 5.67 eV in (a) and 4.14 eV in (b) at the X–C distance equal to 1.542 Å are relative to the undoped diamond. Lines are a guide for the eye.

Chapter 4

Conclusions

In the presented study, the influence of different dopants and their concentrations on the electronic properties and geometry in doped-diamond systems have been investigated within the framework of the Density Functional Theory. Five dopant atoms, namely aluminium, boron, nitrogen, phosphorus and silicon, were considered at three doping concentrations, these being 6.25 %, 1.85 % and 0.78 %. We observed that the interatomic distances between the dopant and the surrounding carbon atoms in the first coordination shell are the same in all the considered cases: the dopant produces an isotropic distortion in the coordination environment, leaving unaltered the symmetries of the pristine system.

According to the band structure calculations, Al, B and Si behave as electron acceptors and induce a narrowing of the band gap. The analysis of the density of states made visible that the band gap is dependent on the concentration of the dopant. A decrease in the concentration causes a widening of the band gap, approaching the value found in the pristine diamond. On the other hand, the band structure of the N- and P-doped systems showed the donor properties of the atomic type of the dopant. We found that, irrespective of the concentration, the diamond structure displays a metallic behaviour when electron donors are used as substituent for the carbon atoms. We also noticed that the larger the distance between the dopant and its first neighbours, the narrower the band gap at constant concentration. On the contrary, an increased dopant-carbon distance produces a widening of the band gap at constant atomic type. Such distance is indeed a convenient descriptor to parameterize the band gap especially when comparing among structures at different doping concentrations and containing the same kind of dopant.

The present thesis provides the starting point for further studies on doped diamond structures, which will lead to the production of manuscripts to be published in impacted scientific journals; indeed, this is what I already planned as a continuation of the present work. Finally, the whole effort has also didactic and motivational implications, since it provided me the basic knowledge on quantum mechanics and the related computational methods and software packages, together with the skills to efficiently exploit high-performance computing facilities.

Appendix A

Bibliography

[AF05] Peter Atkins and Ronald Friedman, *Molecular quantum mechanics*, Oxford University Press Inc., 2005.

[Bec93] Axel D. Becke, *A new mixing of hartree–fock and local density-functional theories*, The Journal of Chemical Physics **98** (1993), no. 2, 1372–1377.

[BO27] M. Born and R. Oppenheimer, *Zur Quantentheorie der Molekeln*, Annalen der Physik **389** (1927), no. 20, 457–484.

[BSW+14] Niels Bindzus, Tine Straasø, Nanna Wahlberg, Jacob Becker, Lasse Bjerg, Nina Lock, Ann-Christin Dippel, and Bo B. Iversen, *Experimental determination of core electron deformation in diamond*, Acta Crystallographica Section A **70** (2014), no. 1, 39–48.

[DS99] C. David Sherrill and Henry F. Schaefer, *The configuration interaction method: Advances in highly correlated approaches*, Advances in Quantum Chemistry, vol. 34, Academic Press, 1999, pp. 143 – 269.

[ETPG16] D. Eon, A. Traoré, J. Pernot, and E. Gheeraert, *Recent progress on diamond schottky diode*, 2016 28th International Symposium on Power Semiconductor Devices and ICs (ISPSD), June 2016, pp. 55–58.

[Fey39] R. P. Feynman, *Forces in molecules*, Phys. Rev. **56** (1939), 340–343.

[GAA+20] Xavier Gonze, Bernard Amadon, Gabriel Antonius, Frédéric Arnardi, Lucas Baguet, Jean-Michel Beuken, Jordan Bieder,

François Bottin, Johann Bouchet, Eric Bousquet, Nils Brouwer, Fabien Bruneval, Guillaume Brunin, Théo Cavignac, Jean-Baptiste Charraud, Wei Chen, Michel Côté, Stefaan Cottenier, Jules Denier, Grégory Geneste, Philippe Ghosez, Matteo Giantomassi, Yannick Gillet, Olivier Gingras, Donald R. Hamann, Geoffroy Hautier, Xu He, Nicole Helbig, Natalie Holzwarth, Yongchao Jia, François Jollet, William Lafargue-Dit-Hauret, Kurt Lejaeghere, Miguel A. L. Marques, Alexandre Martin, Cyril Martins, Henrique P. C. Miranda, Francesco Naccarato, Kristin Persson, Guido Petretto, Valentin Planes, Yann Pouillon, Sergei Prokhorenko, Fabio Ricci, Gian-Marco Rignanese, Aldo H. Romero, Michael Marcus Schmitt, Marc Torrent, Michiel J. van Setten, Benoit Van Troeye, Matthieu J. Verstraete, Gilles Zérah, and Josef W. Zwanziger, *The abinit project: Impact, environment and recent developments*, Comput. Phys. Commun. **248** (2020), 107042.

[Gia92] C. Giacovazzo, *Fundamentals of crystallography*, Oxford University Press Inc., 1992.

[IHTW04] J Isberg, J Hammersberg, D.J Twitchen, and A.J Whitehead, *Single crystal diamond for electronic applications*, Diamond and Related Materials **13** (2004), no. 2, 320 – 324, Carbon Materials for Active Electronics. Proceedings of Symposium L, E-MRS Spring Meeting 2003.

[JA16] P.G. Jambrina and J. Aldegunde, *Chapter 20 - computational tools for the study of biomolecules*, Tools For Chemical Product Design (Mariano Martín, Mario R. Eden, and Nishanth G. Chemmangattuvalappil, eds.), Computer Aided Chemical Engineering, vol. 39, Elsevier, 2016, pp. 583 – 648.

[Kit71] C. Kittel, *Introduction to solid state physics*, John Wiley & Sons Inc., 1971.

[KS65] W. Kohn and L. J. Sham, *Self-Consistent Equations Including Exchange and Correlation Effects*, Physical Review **140** (1965), no. 4A, 1133–1138.

[Kum03] HG Kummel, *A biography of the coupled cluster method*, vol. 17, 11 2003, pp. 5311–5325.

[MI11] Koichi Momma and Fujio Izumi, *VESTA3 for three-dimensional visualization of crystal, volumetric and morphology data*, Journal of Applied Crystallography **44** (2011), no. 6, 1272–1276.

[MP34] Chr. Møller and M. S. Plesset, *Note on an Approximation Treatment for Many-Electron Systems*, Physical Review **46** (1934), no. 7, 618–622.

[MP76] Hendrik J. Monkhorst and James D. Pack, *Special points for brillouin-zone integrations*, Phys. Rev. B **13** (1976), 5188–5192.

[SBv+11] T.P. Straatsma, E.J. Bylaska, H.J.J. van Dam, N. Govind, W.A. de Jong, K. Kowalski, and M. Valiev, *Chapter 7 - advances in scalable computational chemistry: Nwchem*, Annual Reports in Computational Chemistry (Ralph A. Wheeler, ed.), Annual Reports in Computational Chemistry, vol. 7, Elsevier, 2011, pp. 151 – 177.

[SC10] Wahyu Setyawan and Stefano Curtarolo, *High-throughput electronic band structure calculations: Challenges and tools*, Computational Materials Science **49** (2010), no. 2, 299 – 312.

[Sch26] E. Schrödinger, *An undulatory theory of the mechanics of atoms and molecules*, Phys. Rev. **28** (1926), 1049–1070.

[SMG+12] Péter G. Szalay, Thomas Müller, Gergely Gidofalvi, Hans Lischka, and Ron Shepard, *Multiconfiguration self-consistent field and multireference configuration interaction methods and applications*, Chemical Reviews **112** (2012), no. 1, 108–181, PMID: 22204633.

[SMH+14] Alexandrina Stoyanova, Alexander O. Mitrushchenkov, Liviu Hozoi, Hermann Stoll, and Peter Fulde, *Electron correlation effects in diamond: A wave-function quantum-chemistry study of the quasiparticle band structure*, Phys. Rev. B **89** (2014), 235121.

[WB08] Chris J.H. Wort and Richard S. Balmer, *Diamond as an electronic material*, Materials Today **11** (2008), no. 1, 22 – 28.

[WC06] Zhigang Wu and R. E. Cohen, *More accurate generalized gradient approximation for solids*, Phys. Rev. B **73** (2006), 235116.

[Wik07] Wikipedia, the free encyclopedia, *Cubic, face-centered*, 2007, [Online; accessed May 10, 2020].

BACHELOR'S THESIS ASSIGNMENT

I. Personal and study details

Student's name: **Kaintz Matúš** Personal ID number: **474677**

Faculty / Institute: **Faculty of Electrical Engineering**

Department / Institute: **Department of Control Engineering**

Study program: **Cybernetics and Robotics**

II. Bachelor's thesis details

Bachelor's thesis title in English:

Quantum Mechanical Study of Diamond-based Materials for Electronic Applications

Bachelor's thesis title in Czech:

Studie materiálů založených na diamantové bázi pro elektronické aplikace z hlediska kvantové mechaniky

Guidelines:

1) The goal of the present study is to acquire basic knowledge of quantum mechanics and ab initio softwares.
2) As an application, the candidate will study how to engineer the electronic band gap in diamond-based systems. The topic
is in line with the state of the art of the research for new materials for electronic applications. In this respect, diamond has already been recognized to have great potentials in devices such as high-frequency field-effect transistors, high-power switches and Schottky diodes.

Bibliography / sources:

[1] Peter Atkins and Ronald Friedman – Molecular Quantum Mechanics (Fifth Edition) – New York, USA, 2011
[2] Charles Kittel – Introduction to Solid State Physics (Eigth Edition) - New Delhi, India. 2005

Name and workplace of bachelor's thesis supervisor:

Antonio Cammarata, Ph.D., Department of Control Engineering, FEE

Name and workplace of second bachelor's thesis supervisor or consultant:

Date of bachelor's thesis assignment: **06.02.2020** Deadline for bachelor thesis submission: **14.08.2020**

Assignment valid until:
by the end of winter semester 2021/2022

Antonio Cammarata, Ph.D.	prof. Ing. Michael Šebek, DrSc.	prof. Mgr. Petr Páta, Ph.D.
Supervisor's signature	Head of department's signature	Dean's signature

III. Assignment receipt

The student acknowledges that the bachelor's thesis is an individual work. The student must produce his thesis without the assistance of others, with the exception of provided consultations. Within the bachelor's thesis, the author must state the names of consultants and include a list of references.

.	
Date of assignment receipt	Student's signature